Interaction of C 60 Derivatives and ssDNA from Simulations

ARTICLE *in* THE JOURNAL OF PHYSICAL CHEMISTRY C · JUNE 2008

Impact Factor: 4.77 · DOI: 10.1021/jp801180w

Interaction of C_{60} derivatives and ssDNA from simulations

Xiongce Zhao
Center for Nanophase Materials Sciences, Oak Ridge National Laboratory, Oak Ridge, Tennessee 37831, USA
(Dated: February 6, 2008)

We report atomistic modeling studies on the interaction of water-soluble C_{60} derivatives and single stranded DNA (ssDNA) segments in phosphate buffered solutions. Stable hybrids are formed by C_{60} derivatives and ssDNA segments, with binding energies in the range of -23 to -47 kcal/mol. By contrast, the typical binding energy between two C_{60} derivative molecules is -11 to -15 kcal/mol. The binding pattern of C_{60} derivatives with ssDNA molecules depends on the size and shape of the C_{60} functional groups. For C_{60} derivatives with functional group that contains aromatic rings, strong π stacking were observed between the ssDNA base rings and the functional benzene rings. For C_{60} derivatives with a long hydrophilic chain, the binding is greatly enhanced by the hydrophilic interaction from the entanglement between the chain and the ssDNA backbone. Stable hydrogen bonds were observed between the hydroxyl hydrogen on the functional chain and the phosphate oxygen on the ssDNA backbone. For C_{60} derivative with short hydrophilic groups, at least two binding patterns were observed, one of which is dominated by the hydrophobic interaction between the C_{60} surface and bases on ssDNA, and the other involves multiple weak hydrogen bonds between the functional carboxylic groups and ssDNA.

I. INTRODUCTION

The fullerenes were first discovered in 1985[1] and isolated in bulk in 1990[2]. Production of C_{60} on an industrial scale has been successfully realized soon after[3]. Extensive amount of research work have been carried out since then looking for practical applications of these novel materials. In particular, the C_{60}, as the most representative fullerene, has attracted numerous research attentions among communities ranging from material chemistry, biology, to pharmacy. Due to their appealing properties such as the size, hydrophobicity, high cohesivity[4,5], photoactivity[6], and electronic effects[7], C_{60} and its derivatives have aroused great interest in medicinal chemistry[8]. For example, it was discovered that functionalized fullerenes can be used in photodynamic therapy[9] or as inhibitors of the HIV-1 protease[10,11].

One major obstacle for C_{60} application in biological systems is its low solubility in aqueous or polar solvents[12]. Several different approaches can be used to increase the solubility. The first is to encapsulate C_{60} into solubilizing agents such as cyclodextrins[13] or calixarenes[14,15], and to solubilize them in water. The second is to suspend the molecules into water with the help of co-solvents such as benzene and tetrahydrofuran[16]. The third one is to introduce hydrophilic function groups such as amino or hydroxyl groups[17]. C_{60} has been known to have relatively high reactivity that allows various structural modifications[18,19]. Therefore, the last approach serves as a versatile methodology that leads to a wide variety of C_{60} derivatives with different physical and chemical properties[18,20].

From the beginning of the research on the C_{60} and C_{60} derivatives in biological and medical application, there has been a concern about the adverse effects of these molecules. Toxicity was the primary concern. Though earlier studies on C_{60} itself suggested low toxicity[21], it was unclear if water-soluble fullerenes are also innocuous molecules. The pharmacokinetic studies have shown that organofullerenes are excreted either slowly or rapidly, depending on the substituents[22]. Other studies suggest that certain C_{60} derivatives with carboxylic acid groups do not show acute toxicity[23,24]. However, more recent studies suggest that fullerenes may induce oxidative stress in the brain of juvenile largemouth bass[25], and that certain type of C_{60} derivatives show severe toxicity in cell membrane[26]. It was also found that C_{60} can produce heavy disfunctions to the embryo morphogenesis in pregnant mice[27].

Studies on the long term toxicity of C_{60} have so far not been reported. In particular, it is unclear if C_{60} molecules can enter the cell to interact with the most important genetic molecules, DNA. Investigations have been carried out to study the interaction of C_{60} molecules with DNA solutions. For example, experimental studies of C_{60} derivatives with DNA molecules have shown that C_{60} modified with nucleotides can bind to the target DNA and cleave the double strand[28]. Studies were also attempted to use functionalized fullerenes as gene delivery agent[29], since it was found that attachment of C_{60} to DNA causes aggregate formation in a buffer solution. In a previous theoretical study[30], we reported the stable hybrids formed by C_{60} and DNA when C_{60} molecules are docked into the hydrophobic sites of DNA molecules. This suggests that excess exposure to the C_{60} molecules may impact the long term functions of DNA since docked C_{60} molecules can potentially affect the regular duplication or self repair of DNA helix.

Despites these studies, fundamental understandings of how a typical C_{60} derivative interacts with a gene segment at a molecular level still remain as open questions. Given the complexity of the systems of interest, it is challenging to probe these properties by experiment. A promising alternative approach is theoretical modeling, which has been prevalent in recent decades in studying biological systems. Molecular modeling can provide in-

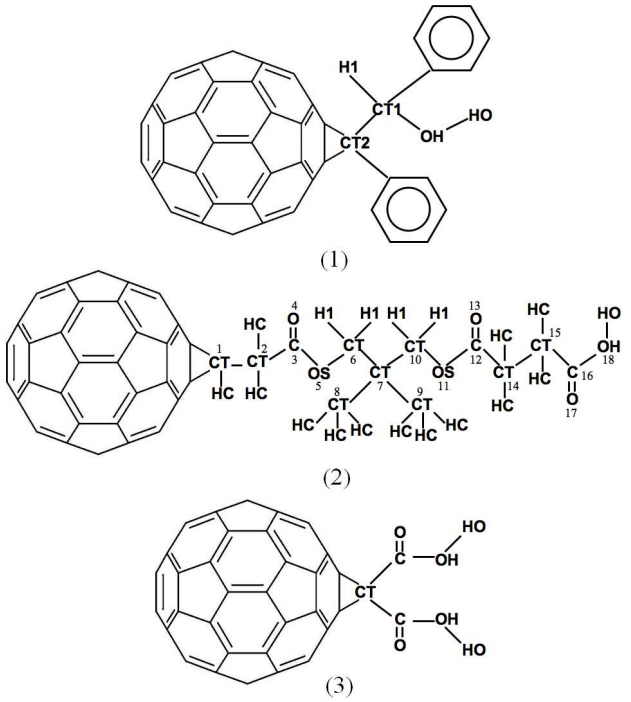

FIG. 1: C_{60} derivatives investigated in this study, denoted as compound 1, 2, and 3 from top to bottom.

sight to questions exposed in experiments, as well as predict useful candidates for targeted applications. For example, the knowledge of interactions between fullerenes and biomolecules is useful in preliminary screening of potential candidates in biomedical applications of interest. One can also use simulation to search for or design better functionalized C_{60} molecules. In this study, we attempt to investigate the interaction of water-soluble C_{60} derivatives and DNA segments in buffered solution through molecular modeling, aiming at a better understanding of the fundamental properties of such bio-nano systems.

II. SIMULATION METHODS

The water-soluble C_{60} derivatives selected in this study are shown in Fig. 1. These three compounds represent some of the most commonly seen C_{60} derivatives synthesized and studied in the past two decades[20]. Each of these compounds contains one to several hydrophilic functional groups. Compound 1 has one hydroxyl group and two benzene rings. Compound 2 is a mono-carboxylic acids with a polyether chain that consists of two carbonyl groups, two ether groups, and an acid group at the end. Compound 3 is a di-carboxylic acid with two -COOH groups connected to the C_{60} surface. In this study, we focus on understanding the physical interaction between the C_{60} derivatives and DNA. This is warranted by the facts that a simple carboxylic acid such as compound 1-3 is unlikely to react chemically with DNA molecules[31].

The single strand DNA used in this study consists of 32 bases, which is composed of eight consecutive repeats of A-G-T-C (poly$(AGTC)_8$). In a typical simulation, the ssDNA and five buckyballs (or their derivatives) were solvated in a pre-equilibrated TIP3P[32] water box consisting of about 22000 water molecules, six KH_2PO_4 molecules (six K^+ ions plus six $H_2PO_4^-$ ions), 10 Na_2HPO_4 molecules (20 Na^+ plus 10 HPO_4^{2-} ions), and 580 NaCl molecules (580 Na^+ ions plus 580 Cl^- ions). The ratios between the number of water molecules and the number of various types of ions added in the system conform to the composition of the phosphate-buffered saline (PBS) solution at 300 K. Additional 31 K^+ counter ions are added to electrically neutralize the negative charges from DNA. Periodic boundary conditions are applied in all three directions. Initial configurations were obtained by placing the C_{60} derivatives along the DNA backbone. The nearest initial distance between any C_{60} molecule and DNA surfaces was about 9 Å, which is within the Lennard-Jones (LJ) cutoff distance used in the simulation.

The DNA and Na^+, Cl^-, K^+ ions were modeled by the CHARMM22 force field[33]. The phosphate ions were modeled by CHARMM22 plus the partial charges derived from a recent first principle calculation[34]. The force field parameters (bonds, angles, dihedrals, LJ parameters, partial charges) for the C_{60} and its derivatives were adopted from the existing CHARMM22 atom types and interaction parameters, as has been done previously[35]. The LJ interaction parameters between different atoms were calculated by the standard Lorentz-Berthelot combing rules, $\sigma_{ij} = (\sigma_i + \sigma_j)/2$ and $\varepsilon_{ij} = (\varepsilon_i \varepsilon_j)^{1/2}$. The cutoff distance for LJ interactions was 1.0 nm with smooth shift, and atom based pair-list with 1.2 nm were updated during the simulation. TIP3P water model was chosen based on previous simulation works[36,37]. The particle-mesh Ewald method with a fourth order interpolation and direct space tolerance of 10^{-6} was applied to evaluate electrostatic interactions. Additional potential parameters can be found in the Supporting Information as well as in the original literature[33].

Molecular dynamics (MD) simulations were performed within the constant pressure (1 bar) and constant temperature (300 K) ensemble[38]. The NAMD[39] software package was employed to integrate the equations of motion. Each simulation included 10000 steps of energy minimization using a conjugate gradient algorithm, followed by gradual heating from 0 to 300 K in 3 ps, solvent equilibration for 5 ps with the DNA backbone atoms constrained, and equilibration of 100 ps without any constraints. Typical production simulations lasted up to 15 ns. The integration time step chosen was two fs. The SHAKE algorithm[40] was applied to constrain the bonds involving hydrogen atoms. The structural configurations were saved every 1 ps for subsequent analysis. Visualizations and analysis were performed using the VMD[41] software package.

III. RESULTS AND DISCUSSIONS

The association of C_{60} compounds and ssDNA segments is characterized by the binding energy for the formation of C_{60}-DNA hybrids. The binding energy between a pair of molecules is defined as[30]

$$\Delta E = E_{\mathrm{A+B}} - E_{\mathrm{A}} - E_{\mathrm{B}} - \Delta E_{\mathrm{deform}},$$

where $E_{\mathrm{A+B}}$, E_{A}, and E_{B} represent the potential energies of the bound A+B pair, molecule A in the bound pair, and molecule B in the bound pair, respectively. $\Delta E_{\mathrm{deform}}$ denotes the deformation energy of the binding molecules. For ssDNA, the deformation can be significant during the association. Therefore, the deformation energy can not be neglected. We define $\Delta E_{\mathrm{deform}}$ as

$$\Delta E_{\mathrm{deform}} = (E_{\mathrm{A}} - E_{\mathrm{A}}^0) + (E_{\mathrm{B}} - E_{\mathrm{B}}^0),$$

where E_{A}^0 and E_{B}^0 represent the potential energy of molecule A and B calculated from simulations without the presence of their binding pairs in the solution. The energetic information was calculated from the post-simulation analysis of the trajectories collected. The energies were obtained by averaging the energetics computed from each frame.

A. C_{60} and DNA

We have simulated the binding of two C_{60} molecules in PBS solution. We found that the binding energy of two C_{60} in PBS solution is consistent with that from our previous study[30], $\Delta E = -7.2$ kcal/mol. This indicates that the presence of the excess salt ions has negligible impact on the association of two C_{60} in the solution.

Simulations of C_{60} and DNA in PBS solution were performed to compare with the findings in our previous study[30]. We found that buckyballs can bind to ssDNA to form stable hybrid in PBS solution. Typically, the binding of C_{60} with ssDNA occurs within about 2 ns. Compared with the previous study[30], the new simulation results indicate that the existence of phosphate ions and large amount of salt ions in the system does not affect the hydrophobic nature of buckyball-DNA interaction. One stabilized binding configuration is illustrated by the snapshot in Fig. 2. The two bound buckyballs shown in the picture are numbered as 1 and 2 from the bottom of the picture. The association of C_{60} 1 with the ssDNA occurred at t=0.9∼1.0 ns, and C_{60} 2 bound to the DNA at about t=2.2 ns.

The binding energies for C_{60} 1 and 2 were found to be −22.8 kcal/mol, −24.4 kcal/mol, respectively. These values are slightly different from those obtained in our previous study in infinitely diluted aqueous solution, but in the similar range. We observed two different binding processes for buckyball 1 and 2. Buckyball 1 associated to the ssDNA by pushing apart two base planes on two neighboring nucleotides, T15 and C16, and then docked inside the two bases. Buckyball 2 was first attracted into a palm-shape hole formed by four consecutive nucleotides G10-T11-C12-A13, and was eventually wrapped by bases on C12 and A13 after a few ns relaxation. However, the final binding configurations for the two C_{60} are similar (see Fig. 2).

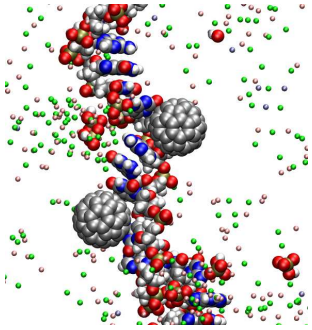

FIG. 2: A snapshot of buckyballs interacting with a ssDNA consisting of 32 bases in PBS solution at 300 K and 1 bar. Atoms in DNA, C_{60}, phosphate ions are in space-fill, salt ions are in small spheres, and water molecules are not shown for clarity. Color scheme: gray(C), red(O), blue(N), yellow(P), white(H), green(Cl^-), pink(Na^+), ice-blue(K^+). The snapshot was taken at t=6.0 ns.

The C_{60}-DNA binding process through "wrapping" by base planes can be seen more clearly in the snapshots and trajectories shown in Fig. 3. Snapshots in Fig. 3(a)-(b) were taken at t=0.9 ns and t=1.0 ns respectively, for the binding of buckyball 1. The base planes of T15 and C16 are roughly parallel before the docking (t=0.9 ns) and changed abruptly to tilting after the bases wrapped the buckyball. The center of mass distance between buckyball 1 and bases T15-C16 drops from 11 Å to about 6.7 Å during the binding process. Correspondingly, the angle between the base planes of T15 and C16 jumped dramatically from nearly parallel to about 100°.

B. Compound 1 and DNA

For comparison purpose, we studied the association of two C_{60} derivatives in PBS solution without the presence of DNA segments and calculated their binding energies. One typical configuration for two bound compound 1 molecules is shown in the snapshot in Fig. 4(a). The initial center of mass distance between the two molecules was 2.2 nm, and their initial interaction energy was zero. After some random movements, two molecules began to attract to each other from t=1.4 ns, with the binding energy went down dramatically. The association process lasted for about 1 ns, until a stable complex is formed at t=2.4 ns, with the benzene rings on their functional groups contacting on the surface of each other (see Fig. 4(a)). The equilibrated bound structure corresponds to a center of mass distance of 0.8 nm between the two molecules, which is about the diameter of C_{60}. The sta-

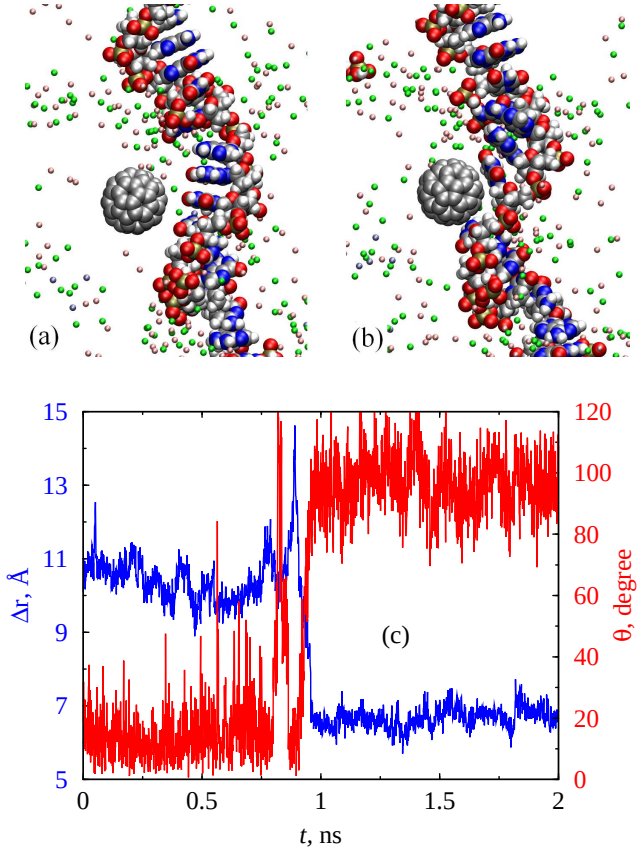

FIG. 3: Docking of C_{60} between two base planes. Snapshots were taken at t=0.9 ns (a) and 1.0 ns (b), respectively. In (c), the red line shows the distance between the buckyball and bases, and the blue line shows the change in the angle between base planes of T15-C16.

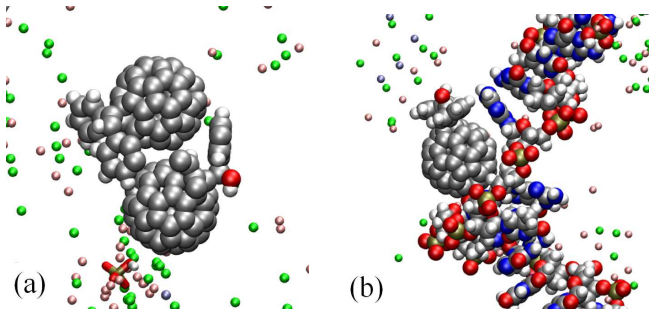

FIG. 4: (a) Association of two compound 1, and (b) binding of compound 1 and ssDNA in PBS solution. The snapshot (a) was taken at time t=8.0 ns during simulation of two compound 1, and the snapshot (b) was taken at t = 11.0 ns during simulations of compound 1 and ssDNA.

bilized binding energy is −10.9 kcal/mol. Thus, the binding of two compound 1 is stronger than that of two native C_{60} in solution due to the additional interaction between the functional groups. The simulation was continued up to 8.0 ns and no disassociation was observed.

It is found from simulations that compound 1 and ssDNA form stable complex in PBS solution. One of the bound structure is given in Fig. 4(b). In this example, the initial center of mass distance between the compound 1 molecule and ssDNA was 1.2 nm. The first contact between them occurred at about t=2 ns. A stable complex formed after that, with a binding energy of −40.2 kcal/mol. The hybrid remains stable within 11 ns of simulation. The binding pattern between compound 1 and ssDNA is slightly different from that for a native C_{60} and ssDNA. Instead of fitting directly into two base planes of ssDNA like a native C_{60} does, compound 1 is wrapped by three consecutive nucleotides due to its relatively larger size by docking into the palm-shape hole formed by the three bases. Its hydrophobic surface contacts with the base planes, while its functional hydrophilic groups either reach into the solution (Fig. 4(b)) or contact with adjacent bases (Fig. 5(a)).

Examination of the binding energy term by term indicates that the binding of compound 1 and DNA is dominated by the hydrophobic forces, like that for a native C_{60} and ssDNA molecules. This is indicated by the fact that the contribution of van der Waals dispersion energy to the total binding energy is typically greater than 90%. Part of the van der Waals energy is from the interaction between the C_{60} surface and bases wrapping it, the rest is from the interaction between a functional benzene ring on the compound and a base plane in ssDNA, which is discussed below.

One distinct feature about the binding of compound 1 and ssDNA is the π-π interaction between the benzene rings in the functional group and the base rings on the ssDNA. π stacking has been found to be a major driving force between the interaction of aromatic buckyball catcher and C_{60}[42]. Interestingly, we also observed very strong π stacking association between compound 1 and ssDNA. One of such observations is depicted in the snapshot shown in Fig. 5 (a). It is seen that one of the benzene rings in the functional groups of the C_{60} derivative stacks with the base plane of G26. The stacking pattern is very similar to that seen between two neighboring bases on DNA molecules. To examine this phenomenon carefully, we monitored the evolution of two parameters that were used to describe the stacking feature, i.e. the distance between the involved benzene plane and G26 base plane, d, and the angles formed by the two planes, γ. Plots of these two parameters as a function of simulation time is given in Fig. 6. The value of d drops dramatically from random to 3.3 Å when the compound binds to the ssDNA at 2.0 ns. Simultaneously, the angle γ between the benzene and base planes goes from random to near zero. The stabilized d of 3.3 Å is same as the distance between two neighboring basepair planes in a standard B-DNA. Simulation was continued up to 11 ns. It can be seen that d and γ remained around their stabilized values except some fluctuations during 5-8.5 ns, suggesting the π stacking observed is fairly stable. Further analysis indicates that the hydrophobic π stacking interaction contributes more than 25% of the total binding energy in

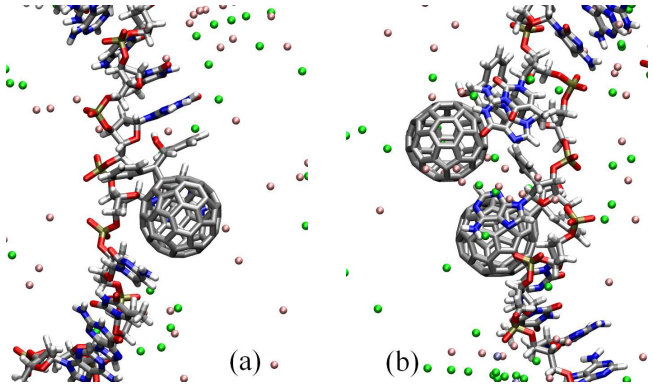

FIG. 5: (a) π stacking interaction between compound 1 and ssDNA, and (b) co-association of two C_{60} derivatives compound 1 on ssDNA in PBS solution.

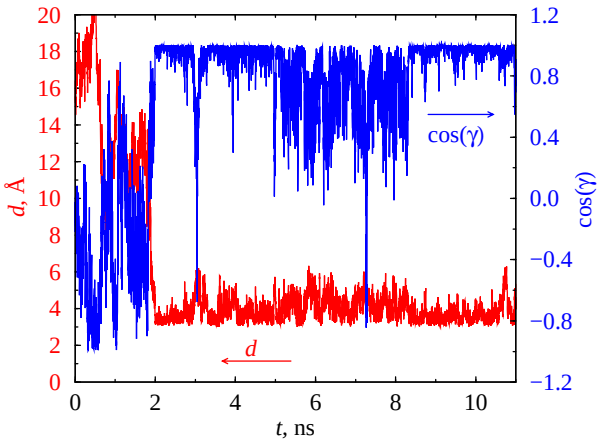

FIG. 6: Distance (red) and angle (blue) between the benzene ring on compound 1 and the G26 base plane of ssDNA.

this case.

Co-adsorption of two compound 1 on ssDNA was also observed. One example structure is presented in the snapshot showing in Fig. 5(b). In this case, two compound 1 molecules that adhered to each other were able to bind together to ssDNA. The overall binding feature exhibited is that two C_{60} derivatives are wrapped by a palm formed by four consecutive nucleotides in the ssDNA molecule, with C_{60} surfaces in contact with the base planes involved. However, when the co-adsorption occurs, we have not observed clear evidence of π stacking like those seen in single-compound-1-ssDNA binding.

C. Compound 2 and DNA

Simulation of C_{60} derivative compound 2 and ssDNA in PBS solution was performed for up to 12 ns. We found that compound 2 can also bind with ssDNA to form stable structures in nanoseconds time scale. However, interaction of compound 2 and ssDNA is qualitatively different from that of compound 1. Compound 2 owns a long chain functional group with a carboxylic tail. This enables it to interact with the hydrophilic ssDNA backbones with more flexibility and thus results in a structure with higher binding energy. One typical snapshot of the hybrid formed by compound 2 and ssDNA is shown in Fig. 7 (a). It can be seen that the C_{60} part of the compound is wrapped by bases on A21-G22-T23, while the functional chain is entangled with the backbone of the ssDNA. In this example, the stabilized hybrid structure corresponds to a binding energy of -47.4 kcal/mol, which is stronger than that of compound 1 binding. In comparison, the binding energy of two compound 2 in PBS solution calculated from simulation is -15.2 kcal/mol.

Breaking down the binding energy term by term indicates that the hydrophilic interaction from the entanglement between functional chain and ssDNA backbone plays an important role in the total binding. Taken the structure in Fig. 7(a) as an example, the binding between the functional chain and ssDNA backbone contribute about 50% of the total energy.

One particular binding feature for compound 2 and ssDNA is the hydrogen bonds formed by the carboxylic group at the end of the functional chain and the phosphate oxygen atoms on the ssDNA backbone. In order to examine this phenomena, we have monitored two geometric parameters that were used to define the hydrogen bond, namely, the distance between the hydrogen atom and the acceptor, and the angle between the donor, the hydrogen, and the acceptor[43]. One example is given in Fig. 8, as the distance h between the H atom (HO in Fig. 1(2), denoted as Compound2:HO) in the ending hydroxyl group of the functional hydrophilic chain in compound 2, and the one of the phosphate O atom (denoted as G22:O1P) in the backbone of nucleotide G22, as well as the angle ϕ between the donor oxygen (OH in Fig. 1(2), denoted as Compound2:OH), Compound2:HO, and G22:O1P. It is seen that h and ϕ fluctuate randomly before the binding occurs. At about t=6.8 ns, h suddenly drops to 1.7 Å, which is the typical length of a hydrogen bond, and ϕ goes up to about 180°, corresponding to the formation of a hydrogen bond between these two atoms. They remain at 1.7 Å and 180° afterward, except a temporary increase/decrease during 8.6-8.8 ns. The standard deviation of h was calculated to be less than 0.1 Å during t=6.8-8.6 ns, which indicates that the hydrogen bond formed is very stable. A snapshot showing the hydrogen bond Compound2:OH$\cdots$O1P:G22 is given in Fig. 7 (b).

D. Compound 3 and DNA

Simulations were performed to study the association between two compound 3 molecules, as well as the binding between compound 3 and ssDNA. The binding energy between two compound 3 is found to be -11.7 kcal/mol in PBS solution without ssDNA. Such a self binding energy is comparable to that of compound 1, but smaller

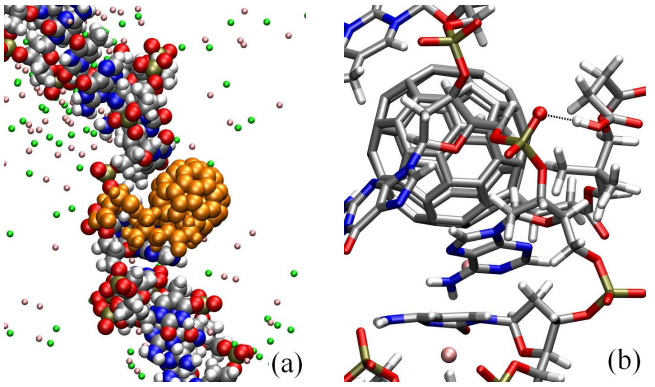

FIG. 7: (a) The hybrid structure formed by C_{60} derivative compound 2 and ssDNA in PBS solution, and (b) the hydrogen bond between the HO atom on the functional chain of compound 2 and a phosphate O on ssDNA backbone. The snapshot (a) shows the final structure after 11 ns of simulation, with the C_{60} derivative colored in orange for clarity, and the hydrogen bond is shown by the dashed line in (b).

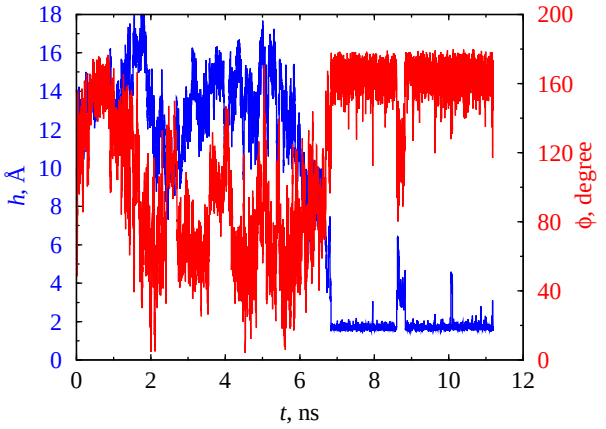

FIG. 8: Formation of the hydrogen bond between the functional group of compound 2 and the backbones of ssDNA. h is the distance between the hydrogen and acceptor oxygen (blue line), ϕ is the angle between the donor, H, and the acceptor (red line), shown as a function of simulation time.

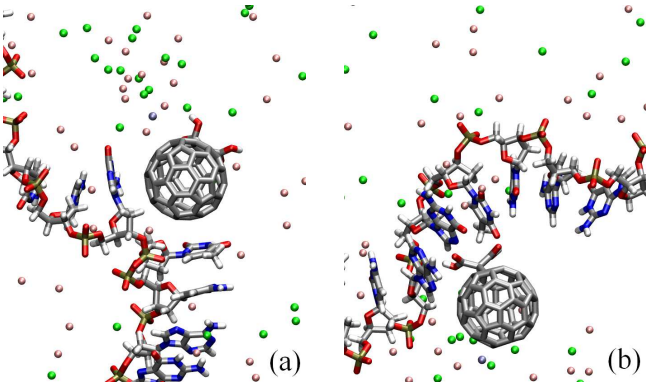

FIG. 9: Two binding patterns between compound 3 and ssDNA. In (a), compound 3 is wrapped by two consecutive base planes on nucleotides G10 and T11. In (b), compound 3 is bound to the edges of the nucleotide G18 and T19 by hydrogen bonding.

than that of compound 2.

At least two binding patterns were observed in compound 3 and ssDNA simulations, which are presented by the snapshots in Fig. 9. In one case, the compound 3 docks into a palm formed by two neighboring bases, with the hydrophilic functional group extending into the solvent, as shown by Fig. 9 (a). This pattern is similar to the pattern observed for compound 1 binding with the ssDNA (Fig. 4(b)) and results in a binding energy of −23.0 kcal/mol. The dominant interaction is the hydrophobic force between the C_{60} part of the derivative and the base planes. The other pattern involves the association of the functional group with the bases, as seen in Fig. 9(b), giving a binding energy of −22.7 kcal/mol. In this case the major interaction is from the hydrogen bonding between the functional groups of the compound and the nucleotides, which will be discussed later. However, the binding energies for these two patterns are essentially the same if simulation fluctuations is taken into account, although the interaction mechanisms are different. In our simulations we did not observe simultaneous occurrence of the two binding patterns for one single compound 3. Compared with the entanglement of compound 2 with ssDNA backbone, the relatively short functional group on compound 3 inhibits it to adapt to an orientation for the two binding patterns to happen simultaneously.

Similar to the binding between compound 2 and ssDNA, compound 3 was also able to form hydrogen bonds with ssDNA. At least two types of hydrogen bonds were observed. The first type is between the carbonyl oxygen on the functional group (such as O1, see Fig. 1 for definitions) and the hydrogen atoms on DNA bases (such as H41 and H42), as shown in Fig. 10(a). The other type is similar to that found in compound 2 and ssDNA interaction, which is between the hydroxyl hydrogen (such as HO2) on compound 3 and the phosphate oxygen on DNA backbones, as shown in Fig. 10(b). In these two kinds of hydrogen bonds, the functional groups on compound 3 serve as proton acceptor and donor, respectively.

However, it is found that the multiple hydrogen bonds between compound 3 and ssDNA are not as stable as the ones observed in compound 2 and ssDNA. This is indicated by the stability of bond lengths, or the O···H distances involved, during the simulations. To give an example, the evolution of two first type hydrogen bonds Compound3:HO2···A17:O1P and Compound3:HO2···G18:O2P are shown in Fig. 11. The lengths of these two hydrogen bonds are plotted as a function of simulation time. It can be seen that hydrogen bond Compound3:HO2···G18:O2P occurred at 0.5, 10.3, and 10.7 ns, respectively, but was interrupted soon afterward. The hydrogen bond Compound3:HO2···A17:O1P was formed during 7-8.5 ns and lasted for a relatively

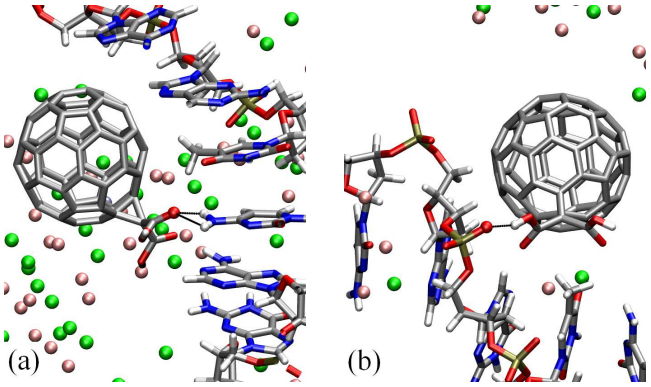

FIG. 10: (a) Formation of hydrogen bonds between the hydrogen atoms H41 and H42 on C20 of ssDNA and the carbonyl oxygen atom O1 on compound 3. (b) The hydrogen bonds between HO2 on the hydroxyl group of compound 3 and the phosphate oxygen O2P on the ssDNA backbone. The hydrogen bonds are shown by the black dashed lines. The snapshot (a) was taken at 3.6 ns, and (b) was taken at 11.0 ns. Refer to Fig. 1(3) for definitions of atoms on compound 3.

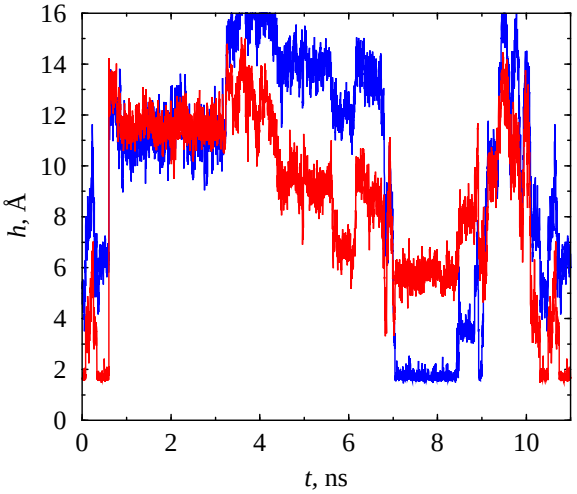

FIG. 11: Hydrogen bonds between HO2 on compound 3 and phosphate oxygen A17:O1P (blue) or G18:O2P (red). The angles between the donor, H, and the acceptor are consitent with the evoluation of h, but not shown in the figure for clarity.

longer time, but was not sustained.

Similar metastability was also observed for the second type of hydrogen bonds between the carbonyl oxygen on compound 3 and the hydrogen atoms on bases. One such example is shown in Fig. 12. Here the hydrogen bonds involve four atoms, which are two carbonyl oxygen atoms O1 and O2 on compound 3 and two hydrogen atoms connected to the N4 atom, H41 and H42, on base C20. H42 can form hydrogen bonds with either O1 or O2, as shown Fig. 12(a). It bonds to O1 during t=3.6-4.0 ns, and switches to O2 during t=4.3-6.8 ns. The O1 atom can form hydrogen bonds with either H41 or H42 and switch

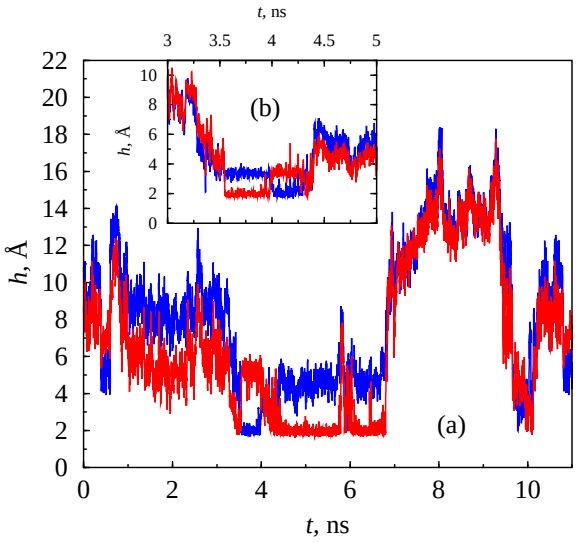

FIG. 12: (a) Hydrogen bond between the C20:H42 atom and the carbonyl oxygen atoms O1 (blue) and O2 (red) on compound 3. (b) Swapping hydrogen bonds between C20:H41(blue)/C20:H42(red) and the carbonyl oxygen O1 on compound 3.

between them during the binding. This is illustrated by the bond length evolution of O1:H42/O1:H42 during 3.6-4.3 ns as shown in Fig. 12(b). Compared with that observed in compound 2, the relatively unstable hydrogen bonds observed for compound 3 are in accordance with a much lower total binding energy.

One possible reason for the intermittent and unstable hydrogen bonds between compound 3 and ssDNA is the lack of coordinating hydrophobic force from C_{60} and bases like that observed in compound 2. As discussed above, relative short functional groups in compound 3 prohibit it from taking an orientation that allows both hydrophobic and hydrophilic interactions with ssDNA. It is plausible that the hydrophobic interaction between C_{60} surface of compound 2 and bases on ssDNA helped to stabilize the hydrogen bond between Compound2:OH and G22:O1P. This is especially true if one takes into account the competition from hydrogen bonds between solute and water molecules.

IV. CONCLUSIONS

In summary, we found from molecular simulations that C_{60} and its derivatives can bind to single strand DNA and form energetically stable hybrids in highly salted buffer solution. The results on the binding of C_{60} with ssDNA are consistent with our previous simulations using a diluted aqueous solution. The binding of hydrophilically functionalized C_{60} derivatives to ssDNA segments has a similar or higher stability than that of native C_{60} molecules.

From standpoint of binding energy, the strongest binding occurred for a C_{60} with a long hydrophilic chain (compound 2). The strong interaction came from two parts of contributions, the hydrophobic force between the C_{60} surface and base planes, and the hydrophilic interaction between the functional group and the DNA backbones through entanglement. This gives a binding energy of about -47 kcal/mol. For C_{60} derivative with benzene rings and hydroxyl group (compound 1), the binding energy is -40 kcal/mol, with part of the interaction from the π stacking between the benzene ring and the base planes of the DNA. The binding of compound 3, which has two short carboxylic acid groups on the surface, gives an essentially same interaction energy as that of native C_{60}. However, at least two different binding patterns were observed for compound 3. In particular, multiple intermittent hydrogen bonds were observed between the carboxylic groups on compound 3 and ssDNA.

The present findings suggest several effects in using C_{60} derivatives in biomedical applications. For instance, simulations in this work indicate that different functional groups on a C_{60} result in different binding strength and binding features with DNA segments. Such information is useful in designing, for example, target-specific gene delivery C_{60} agents by modifications of the functional groups. On the other hand, very strong binding between DNA and certain C_{60} derivatives implies possible adverse effects to the gene. It is unknown if water-soluble C_{60} derivatives in environment can readily enter the cell nucleus. If so, the association of C_{60} derivatives with DNA would be strong enough to impair the regular functioning of the DNA.

In closing, we note that further studies can be performed in several aspects. Firstly, the current results are based on relatively short time scales we are able to model with standard MD. There could be other interesting phenomena occurring well beyond nanoseconds which were not observed in this work. Simulations with much longer timescale is desired, but will demand significant computing powers. Secondly, the energetic information given here is based on binding energy. Instead of binding energy, binding free energy is more of interest for practical applications. One could calculate the free energy of binding between C_{60} derivatives and DNA by computing the potential of mean force associated with binding of the molecule to DNA. However, such an approach requires the identification of a set of conformational coordinates that span the binding process, which is not well defined in C_{60}/DNA interaction. Finally, the binding of C_{60} derivatives with double strand DNA could be another point of interest for future studies.

Acknowledgments

The author thanks Peter T. Cummings for many helpful discussions. This research was conducted at the Center for Nano phase Materials Sciences, which is sponsored at Oak Ridge National Laboratory by the Division of Scientific User Facilities, U.S. Department of Energy. This research used resources of the National Energy Research Scientific Computing Center, which is supported by the Office of Science of the U.S. Department of Energy under Contract No. DE-AC02-05CH11231.

[1] Kroto, H. W.; Heath, J. R.; O'Brien, S. C.; Curl, R. F.; Smalley, R. E. *Nature* **1985**, *318*, 162.
[2] Kratschmer, W.; Lamb, L. D.; Rostiropoulos, K.; Huffman, D. R. *Nature* **1990**, *347*, 354.
[3] Howard, J. B.; McKinnon, J. T.; Makarovsky, Y.; Lafleur, A. L.; Johnson, M. E. *Nature* **1991**, *352*, 139.
[4] Hamza, A. V.; Balooch, M. *Chem. Phys. Lett.* **1993**, *201*, 404.
[5] Deguchi, S.; Alargova, R. G.; Tsuji, K. *Langmuir* **2001**, *17*, 6013.
[6] Guldi, D. M.; Rato, M. *Acc. Chem. Res.* **2000**, *33*, 695.
[7] Martin, N.; Sanchez, L.; Llescas, B.; Perez, I. *Chem. Rev.* **1998**, *98*, 2527.
[8] Da Ros, T.; Prato, M. *Chem. Comm.* **1999**, 663.
[9] Tokuyama, H.; Yamago, S.; Nakamura, E.; Shiraki, T.; Sugiura, Y. *J. Am. Chem. Soc.* **1993**, *115*, 7918.
[10] Friedman, S. H.; DeCamp, D. L.; Sijbesma, R. P.; Srdanov, G.; Wudl, R.; Kenyon, G. L. *J. Am. Chem. Soc.* **1993**, *115*, 6506.
[11] Sijbesma, R.; Srdanov, G.; Wudl, F.; Castoro, J. A.; Wilkins, C.; Friedman, S. H.; DeCamp, D. L.; Kenyon, G. L. *J. Am. Chem. Soc.* **1993**, *115*, 6510.
[12] Korobov, M. V.; Smith, A. L. *Fullerenes: Chemistry, Physics, and Technology*, New York, 2000; pp 53–89.
[13] Diederich, F.; Gomez-Lopez, M. *Chem. Soc. Rev.* **1999**, *28*, 263–277.
[14] Ikeda, A.; Hatano, T.; Kawaguchi, M.; Suenaga, H.; Shinkai, S. *Chem. Comm.* **1999**, *15*, 1403–1404.
[15] Atwood, J. L.; Koutsantonis, G. A.; Raston, C. L. *Nature* **1994**, *368*, 229–231.
[16] Scrivens, W. A.; Tour, J. M.; Creek, K. E.; Pirisi, L. *J. Am. Chem. Soc.* **1994**, *116*, 4517.
[17] Chiang, L. Y.; Upasani, R. B.; Swirczewski, J. W. *J. Am. Chem. Soc.* **1992**, *114*, 10154–10157.
[18] Hirsch, A. *Chemistry of Fullerenes*; Thieme: Stuttgart, 1994.
[19] Diederich, F.; Kessinger, R. *Templated Organic Synthesis*, Weinheim, 2000; pp 189–218.
[20] Nakamura, E.; Isobe, H. *Acc. Chem. Res.* **2003**, *36*, 807–815.
[21] Nelson, M. A.; Domann, F. E.; Bowden, G. T.; Hooser, S. B.; Fernando, Q.; Carter, D. E. *Toxicol. Ind. Health* **1993**, *9*, 623–630.
[22] Tabata, Y.; Murakami, Y.; Ikada, Y. *Jpn. J. Cancer Res.* **1997**, *88*, 11108–11116.
[23] Yamago, S.; tokuyama, H.; Nakamura, E.; Kikuchi, K.;

Kananishi, S.; Sueki, K.; Nakhara, H.; Enomoto, S.; Ambe, F. *Chem. Biol.* **1995**, *2*, 385–389.
[24] Rancan, F.; Rosan, S.; Boehm, F.; Cantrell, A.; Brellreich, M.; Schoenberger, H.; Hirsch, A.; Moussa, F. *J. Photochem. Photobiol. B: Biol.* **2002**, *67*, 157–162.
[25] Oberdörster, E. *Environmental Health Perspectives* **2004**, *112*, 1058.
[26] Bosi, S.; Feruglio, L.; Ros, T. D.; Spalluto, G.; Gregoretti, B.; Terdoslavich, M.; Decorti, G.; Passamonti, S.; Moro, S.; Prato, M. *J. Med. Chem.* **2004**, *47*, 6711.
[27] Tsuchaya, T.; Oguri, I.; Yamakoshi, Y. N.; Miyata, N. *FEBS Lett.* **1996**, *393*, 139.
[28] Boutorine, A. S.; Tokuyama, H.; Takasugi, M.; Isobe, H.; Nakamura, E.; Helene, C. *Angew. Chem. Int. Ed. Engl.* **1994**, *33*, 2462–2465.
[29] Yamakoshi, Y. N.; Yagami, T.; Sueyoshi, S.; Miyata, N. *J. Org. Chem.* **1996**, *61*, 7236–7237.
[30] Zhao, X. C.; Striolo, A.; Cummings, P. T. *Biophysical J.* **2005**, *89*, 3856.
[31] Nakamura, E.; Isobe, H.; Tomita, N.; Sawamura, M.; Jinno, S.; Okayama, H. *Angew. Chem., Int. Ed.* **2000**, *39*, 4254–4257.
[32] Jorgensen, W. L. *J. Am. Chem. Soc.* **1981**, *103*, 335.
[33] MacKerell Jr., A. D. et al. *J. Phys. Chem. B* **1998**, *102*, 3586.
[34] Klähn, M.; Mathias, G.; Kötting, C.; Nonella, M.; Schlitter, J.; Gerwert, K.; Tavan, P. *J. Phys. Chem. A* **2004**, *108*, 6186–6194.
[35] Zhu, Z. W.; Schuster, D. I.; Tuckerman, M. E. *Biochemistry* **2003**, *42*, 1326–1333.
[36] Cheatham III, T. E.; Kollman, P. A. *Annu. Rev. Phys. Chem.* **2000**, *51*, 435.
[37] Cheatham III, T. E.; Young, M. A. *Biopolymers* **2001**, *56*, 232.
[38] Berendsen, H. J. C.; Postma, J. P. M.; van Gunsteren, W. F.; Nola, A. D.; Haak, J. R. *J. Chem. Phys.* **1984**, *81*, 3684.
[39] Kale, L.; Skeel, R.; Bhandarkar, M.; Brunner, R.; Gursoy, A.; Krawetа, N.; Phillips, J.; Shinozaki, A.; Varadarajan, K.; Schulten, K. *J. Comput. Phys.* **1999**, *151*, 283.
[40] Ryckaert, J. P.; Ciccotti, G.; Berendsen, H. J. C. *J. Comput. Phys.* **1977**, *23*, 4613–4621.
[41] Humphrey, W.; Dalke, A.; Schulten, K. *J. Molec. Graphics* **1996**, *14*, 1.
[42] Sygula, A.; Fronczek, F. R.; Sygula, R.; Rabideau, P. W.; Olmstead, M. M. *J. Am. Chem. Soc.* **2007**, *129*, 3842.
[43] Raschke, T. M.; Levitt, M. *Proc. Natl. Acad. Sci.* **2005**, *102*, 6777.

Supporting Information

Interaction of C_{60} derivatives and DNA from simulations

Xiongce Zhao
Center for Nanophase Materials Sciences, Oak Ridge National Laboratory, Oak Ridge, Tennessee 37831, USA

I. SYSTEM SETUP

The single strand DNA used in this study consists of 32 bases, which is composed of eight consecutive repeats of A-G-T-C (poly(AGTC)$_8$), with a head-to-tail length of about 10.5 nm. The single strand DNA segments were obtained by taking one helix from a double B-form helix created using the DNA-RNA building utility software NUCGEN contained in AMBER [1]. In a typical simulation, the ssDNA and five buckyballs (or their derivatives) were solvated in a solvent box which contains about 22000 pre-equilibrated TIP3P [2] water molecules, six KH_2PO_4 molecules (six K^+ ions plus six $H_2PO_4^-$ ions), 10 Na_2HPO_4 molecules (20 Na^+ plus 10 HPO_4^{2-} ions), and 580 NaCl molecules (580 Na^+ ions plus 580 Cl^- ions). The ratios between the number of water molecules and the number of various types of ions added in the system conform to the composition of the phosphate-buffered saline (PBS) solution at 300 K. Additional 31 K^+ counter ions are added to electrically neutralize the negative charges from DNA. A water buffer layer of at least 2.0 nm exists between the solute surface and the boundaries. Totally there are ∼64000 atoms in the simulation cell. The initial size of the simulation box is about 6.3 nm by 7.6 nm by 15.2 nm. The stabilized simulation box volume is 6.1 nm by 7.4 nm by 14.9 nm. Periodic boundary conditions are applied in all three directions. Initial configurations were obtained by placing the C_{60} or C_{60} derivatives along the DNA backbone. The initial distance between a C_{60} and the DNA varies slightly from one C_{60} to another. The nearest initial distance between any C_{60} molecule and DNA surfaces was about 9 Å, which is within the Lennard-Jones cutoff distance. Such a setup permitted a clear separation between the C_{60} and DNA strands at the beginning of the simulations, while maintaining the simulation cell within a computationally manageable size. It is worthwhile to note that the PBS solution composition was set up based on the molecular ratios (water to ions) rather than on the volumetric concentrations because the volume occupied by macromolecules (DNA and buckyballs) in the box is ineligible.

II. FORCE FIELDS

The DNA and Na^+, Cl^-, K^+ ions were modeled by the CHARMM22 force field [3]. The CHARMM22 force field is described by

$$\begin{aligned} U_t = & \sum_{\text{bond}} k_r(r-r_0)^2 + \sum_{\text{angle}} k_\theta(\theta-\theta_0)^2 \\ & + \sum_{\text{dihedral}} \frac{V_n}{2}[1+\cos(n\phi-\gamma)] \\ & + \sum_{i<j} 4\varepsilon_{ij}\left(\frac{\sigma_{ij}^{12}}{r_{ij}^{12}} - \frac{\sigma_{ij}^{6}}{r_{ij}^{6}}\right) + \sum_{i<j}\frac{q_i q_j}{r_{ij}} \end{aligned} \quad (1)$$

The first term in the right hand side is from the bond stretching potential for all the chemical bonds in the system. The second term is from the bond angles. The third term is from the dihedrals. The fourth and fifth terms are the dispersion (van der Waals) and electrostatic interactions between any pair of atoms in different molecules, or any pair of atoms in the same molecule but separated by at least three bonds. The ions were modeled as Lennard-Jones (LJ) particles plus partial charges. The LJ parameters of each type of atoms in Na^+, Cl^-, K^+, $H_2PO_4^-$, and HPO_4^{2-} were from the CHARMM22 potential. The structures and corresponding CHARMM22 atom type for each atom involved in $H_2PO_4^-$ and HPO_4^{2-} ions are shown in Table I and II. The equilibrium molecular configurations and partial charges for the phosphate ions, which are shown in Table II, were from a recent first principle calculations [4]. The force field parameters (bonds, angles, dihedrals, LJ parameters, partial charges) for the C_{60} and its derivatives were adopted from the existing CHARMM22 atom types and interaction parameters, as has been done previously [5]. The LJ interaction parameters between different atoms were calculated by the standard Lorentz-Berthelot combing rules, $\sigma_{ij} = (\sigma_i + \sigma_j)/2$ and $\varepsilon_{ij} = (\varepsilon_i\varepsilon_j)^{1/2}$. The cutoff distance for LJ interactions was 1.0 nm with smooth shift, and atom based pair-list with 1.2 nm were updated during the simulation. TIP3P water model was chosen based on previous simulation works [6, 7]. The particle-mesh Ewald method with a fourth order interpolation and direct space tolerance of 10^{-6} was applied to evaluate electrostatic interactions. Part of the potential parameters for $H_2PO_4^-$, HPO_4^{2-}, C_{60}, and C_{60} derivatives can be found in Table II to VI. Additional potential parameters for each type of atoms, such as angles, bonds, dihedrals, and LJ parameters, can be found in the literature [3].

TABLE I: Structure of HPO_4^{2-} and $H_2PO_4^-$ ions.

	HPO_4^{2-}	$H_2PO_4^-$
Chemical Structure	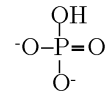	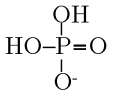
Atom Name	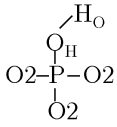	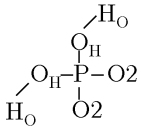

TABLE II: Potential parameters for phosphate ions HPO_4^{2-} and $H_2PO_4^-$. The partial charges (e) are from a recent *ab initio* simulations [4].

	CHARMM22		
Atom Name	Atom Type	$q(HPO_4^{2-})$	$q(H_2PO_4^-)$
P	P2	1.43	1.20
O2(=O)	ON3	−1.02	−0.86
O2(ester O)	ON2	−1.02	−0.86
O_H	OH1	−0.76	−0.64
H_O	H	0.39	0.40

III. SIMULATION DETAILS

Molecular dynamics (MD) simulations were performed within the constant pressure (1 bar) and constant temperature (300 K) ensemble [8]. The NAMD [9] software package was employed to integrate the equations of motion. Each simulation included 10000 steps of energy minimization using a conjugate gradient algorithm, followed by gradual heating from 0 to 300 K in 3 ps, solvent equilibration for 5 ps with the DNA backbone atoms constrained, and equilibration of 100 ps without any constraints. Typical production simulations lasted up to 15 ns. The integration time step chosen was two fs. The SHAKE algorithm [10] was applied to constrain

TABLE III: Molecular mechanical configuration parameters for phosphate ions [4].

Bonds		r_0 [Å]	k_r [kcal/mol/Å^2]
	P−O2	1.610	395
	P−O_H	1.870	98
	O_H−H_O	0.980	519
Angles		θ_0	k_θ [kcal/mol/rad^2]
	O2−P−O2	116°	73
	O2−P−O_H	105°	73
	H_O−O_H−P	105°	45
Dihedrals	γ	n	V_n [kcal/mol]
O2−P−O_H−H_O	0°	3	1.2

TABLE IV: Potential parameters for C_{60} derivative compound 1. The parameters for bonds, angles, dihedrals, and the LJ parameters of each atom were adapted from the corresponding CHARMM22 parameters according the atom type shown. Partial charges for each atom are given in the table

	CHARMM22	
Atom Name	Atom Type	q [$\|e\|$]
C on C_{60}	CA	0.0
CT2	CT	0.0
CT1	CT1	0.14
H1	HB	0.09
OH	OH1	−0.66
HO	H	0.43
C on benzene connected to CT1, CT2	CA	0.0
C on benzene with H	CA	−0.115
H on benzene	HP	0.115

TABLE V: Potential parameters for C_{60} derivative compound 2 (see Fig. 2 for atom numbers).

	CHARMM22	
Atom Number	Atom Type	q [$\|e\|$]
C on C_{60}	CA	0.0
1	CT1	−0.09
2,14	CT2	−0.18
3,12	C	0.73
4,13	O	−0.52
5,11	OS	−0.34
6,10	CT2	−0.05
7	CT	0.0
8,9	CT3	−0.27
15	CT2	−0.21
16	C	0.75
17	O	−0.55
18	OH1	−0.61
H connected to CT	HA	0.09
H connected to CT	HB	0.09
H connected to OH	H	0.44

TABLE VI: Potential parameters for C_{60} derivative compound 3.

	CHARMM22	
Atom Name	Atom Type	q [$\|e\|$]
C on C_{60}	CA	0.0
CT	CT	0.0
C	C	0.75
O	O	−0.55
OH	OH1	−0.64
HO	H	0.44

the bonds involving hydrogen atoms. The structural configurations were saved every 1 ps for subsequent analysis. Visualizations and analysis were performed using the VMD [11] software package.

[1] Case, D. A.; Darden, T. A.; Cheatham III, T. E.; Simmering, C. L.; Wang, J.; Duke, R. E.; Luo, R.; Merz, K. M.; Wang, B.; Pearlman, D. A.; Crowley, M.; Brozell, S.; Tsui, V.; Gohlke, H.; Mongan, J.; Hornak, V.; Cui, G.; Beroza, P.; Schafmerster, C.; Caldwell, J. W.; Ross, W. S.; Kollman. P. A. *AMBER 8.0*, 2004.

[2] Jorgensen, W. L. *J. Am. Chem. Soc.* **1981**, *103*, 335.

[3] MacKerell Jr., A. D.; Bashford, D.; Bellott, M.; Dunbrack Jr., R. L.; Evanseck, J. D.; Field, M. J.; Fischer, S.; Gao, J.; Guo, H.; Ha, S.; Joseph-McCarthy, D.; Kuchnir, L.; Kuczera, K.; Lau, F. T. K.; Mattos, C.; Michnick, S.; Ngo, T.; Nguyen, D. T.; Prodhom, B.; Reiher III, W. E.; Roux, B.; Schlenkrich, M.; Smith, J. C.; Stote, R,; Straub, J.; Watanabe, M.; Wiórkiewicz-Kuczera, J.; Yin, D.; Karplus, M. *J. Phys. Chem. B* **1998**, *102*, 3586.

[4] Klähn, M.; Mathias, G.; Kötting, C.; Nonella, M.; Schlitter, J.; Gerwert, K.; Tavan, P. *J. Phys. Chem. A* **2004**, *108*, 6186–6194.

[5] Zhu, Z. W.; Schuster, D. I.; Tuckerman, M. E. *Biochemistry* **2003**, *42*, 1326–1333.

[6] Cheatham III, T. E.; Kollman, P. A. *Annu. Rev. Phys. Chem.* **2000**, *51*, 435.

[7] Cheatham III, T. E.; Young, M. A. *Biopolymers* **2001**, *56*, 232.

[8] Berendsen, H. J. C.; Postma, J. P. M.; van Gunsteren, W. F.; Nola, A. D.; Haak, J. R. *J. Chem. Phys.* **1984**, *81*, 3684.

[9] Kale, L.; Skeel, R.; Bhandarkar, M.; Brunner, R.; Gursoy, A.; Kraweta, N.; Phillips, J.; Shinozaki, A.; Varadarajan, K.; Schulten, K. *J. Comput. Phys.* **1999**, *151*, 283.

[10] Ryckaert, J. P.; Ciccotti, G.; Berendsen, H. J. C. *J. Comput. Phys.* **1977**, *23*, 4613–4621.

[11] Humphrey, W.; Dalke, A.; Schulten, K. *J. Molec. Graphics* **1996**, *14*, 1.